HHS Public Access

Author manuscript

J Immunol. Author manuscript; available in PMC 2024 March 15.

Published in final edited form as:

J Immunol. 2023 March 15; 210(6): 721–731. doi:10.4049/jimmunol.2200746.

IFN-induced protein with tetratricopeptide repeats 2 (Ifit2) limits autoimmune inflammation by regulating myeloid cell activation and metabolic activity

Dongkyun Kim[*,1], **Nagendra Kumar Rai**[†,1], **Amy Burrows**[‡], **Sohee Kim**[*], **Ajai Tripathi**[†], **Samuel E. Weinberg**[¶], **Ranjan Dutta**[†], **Ganes C. Sen**[‡], **Booki Min**[*]

[*]Department of Microbiology and Immunology, Northwestern University Feinberg School of Medicine, Chicago, IL 60611.

[†]Department of Neuroscience, Lerner Research Institute, Cleveland Clinic Foundation, Cleveland, OH 44195.

[‡]Department of Inflammation and Immunity, Lerner Research Institute, Cleveland Clinic Foundation, Cleveland, OH 44195.

[¶]Department of Pathology, Northwestern University Feinberg School of Medicine, Chicago, IL 60611.

Abstract

Besides anti-viral functions, Type I IFN expresses potent anti-inflammatory properties and is being widely used to treat certain autoimmune conditions, such as multiple sclerosis (MS). In murine model of MS, experimental autoimmune encephalomyelitis (EAE), administration of IFNβ effectively attenuates the disease development. However, the precise mechanisms underlying IFNβ-mediated treatment remain elusive. In this study, we report that IFN-induced protein with tetratricopeptide repeats 2 (Ifit2), a type I and type III IFN-stimulated gene, plays a previously unrecognized immune regulatory role during autoimmune neuroinflammation. Mice deficient in Ifit2 displayed greater susceptibility to EAE and escalated immune cell infiltration in the central nervous system. Ifit2 deficiency was also associated with microglial activation and increased myeloid cell infiltration. We also observed that myelin debris clearance and the subsequent remyelination was substantially impaired in *Ifit2*$^{-/-}$ CNS tissues. Clearing myelin debris is an important function of reparative type myeloid cell subset to promote remyelination. Indeed, we observed that bone marrow derived macrophages, CNS infiltrating myeloid cells, and microglia from *Ifit2*$^{-/-}$ mice express cytokine and metabolic genes associated with proinflammatory type

Address correspondence and reprint requests to Booki Min, Department of Microbiology and Immunology, Northwestern University Feinberg School of Medicine, Chicago, IL 60611. booki.min@northwestern.edu; Ganes Sen, Department of Inflammation and Immunity, Cleveland Clinic Foundation, Cleveland, OH 44195. seng@ccf.org; Ranjan Dutta, Department of Neuroscience, Cleveland Clinic Foundation, Cleveland, OH 44195. duttar@ccf.org.

[1]These authors contributed equally

Author Contributions

DK, RD, GCS, and BM conceived the study; DK, NKR, AB, SK, AT, and SEW performed experiments; RD, GCS, and BM wrote the manuscript; DK, NKR, RD, GCS, and BM edited the manuscript; and BM supervised the study.

Conflicts of Interest

The authors have declared that no conflicts of interest exist.

myeloid cell subsets. Taken together, our findings uncover a novel regulatory function of Ifit2 in autoimmune inflammation in part by modulating myeloid cell function and metabolic activity.

Introduction

Type I IFN (IFN-I) is widely used to treat acute and chronic inflammation including autoimmunity in the central nervous system (CNS), especially multiple sclerosis (MS) (1–4). Despite its broad applications, the precise mechanisms by which IFN-I elicits its treatment effects within the CNS remain largely unclear. IFNβ administration ameliorates the severity of experimental autoimmune encephalomyelitis (EAE), an animal model for human multiple sclerosis (5, 6). IFN-I is also induced within the CNS during EAE, and it was reported that endogenously produced IFN-I plays a key role in regulating EAE pathogenesis, since mice deficient in IFN-I receptor (IFNAR) or in TIR domain-containing adaptor-inducing interferon β (TRIF), a cytosolic adaptor molecule needed to induce IFN-I production, develop exacerbated EAE (7, 8). The use of cell type specific *Ifnar*$^{-/-}$ mice further uncovers that IFN-I signaling in T cells or neurons is dispensable and that the signaling in myeloid cells is essential for the anti-inflammatory function of endogenously produced IFN-I (7). Nevertheless, the cellular and molecular mechanisms by which endogenously produced IFN-I mediates its anti-inflammatory functions remain largely unknown.

IFN-I orchestrates both innate and adaptive immunity by inducing IFN stimulated genes (ISGs) in multiple cell types (9, 10). IFN-induced tetratricopeptide repeats (Ifit) is a group of ISG protein family consisted of 4 families in human (3 families in mice, IFIT1/ISG56, IFIT2/ISG54, and IFIT3/ISG60). Ifit proteins play important anti-viral roles through their ability to bind viral RNA and to interfere with translation (11–13). The anti-viral functions of Ifit overlap amongst the Ifit family proteins, although the mechanisms utilized by each Ifit member could be unique and distinct (13–15). We recently reported that Ifit2 protects mice from lethal neurotropic MHV infection (16). Pronounced mortality of *Ifit2*$^{-/-}$ mice during the infection is accompanied by uncontrolled virus replication and spread throughout the brain as well as by significantly impaired microglial activation and reduced recruitment of inflammatory cells to the brain (16). In addition to broad anti-viral functions, Ifit is known to play a diverse regulatory role in immunity. In LPS activated macrophages, Ifit1 not only supports IFN-I expression but also limits the inflammatory gene expression (17). Ifit3 negatively regulates TLR3 induced IFNβ and Cxcl10 expression in human brain endothelial cells (18). However, whether Ifit plays a role in autoimmune inflammation has not previously been examined.

In this study, we report that Ifit2 plays a novel role in limiting autoimmune neuroinflammation. Mice deficient in Ifit2 were highly susceptible to EAE, and inflammatory responses in the CNS tissue were markedly elevated in these mice. Unlike MHV infection, Ifit2 deficiency in EAE was associated with pronounced microglial activation and macrophage infiltration. Interestingly, severely impaired myelin debris clearance and remyelination failure were observed in *Ifit2*$^{-/-}$ CNS tissues. Myelin debris clearance is an important function of reparative phenotype myeloid cells, and we found that infiltrating myeloid cells and microglia express genes and metabolic profiles associated

with proinflammatory phenotype myeloid cells in *Ifit2*$^{-/-}$ mice. Therefore, these results demonstrate that Ifit2 may be a critical ISG that mediates IFN-I's anti-inflammatory functions in autoimmune neuroinflammation by supporting reparative phenotype myeloid cell differentiation and functions, which promote myelin debris clearance and remyelination.

Materials and Methods

Mice

C57BL/6 (B6) mice were purchased from The Jackson Laboratory (Bar Harbor, ME). *Ifit*-whole locus$^{-/-}$ and *Ifit2*$^{-/-}$ mice were previously reported (19, 20). All mouse strains were housed, maintained, and bred under specific pathogen-free conditions at the Northwestern University Feinberg School of Medicine and Lerner Research Institute of Cleveland Clinic Foundation. All experimental procedures with mice were approved by the Institutional Animal Care and Use Committee (IACUC) of the Northwestern University and of the Cleveland Clinic Foundation.

Induction of EAE

Mice were subcutaneously immunized on the back with 300μg of $MOG_{35–55}$ peptide (BioSynthesis, Lewisville, TX) emulsified in equal volume of CFA containing 5 mg/ml Mycobacterium tuberculosis H37Ra (Difco, Detroit, MI). Mice were also injected with 200 ng pertussis toxin (Sigma, St. Louis, MO) intraperitoneally on day 0 and 2 post immunization. EAE development was monitored and graded on a scale of 0 to 5: 0, no disease; 1, limp tail; 2, hind limb weakness; 3, hind limb paralysis; 4, hind and fore limb paralysis; 5, moribund or death.

Real-Time Quantitative PCR (qPCR)

Mice were euthanized at the peak of disease and perfused with cold PBS. Total RNA was extracted from homogenized brains and spinal cords using TRIzol reagent according to the manufacturer's instructions (Invitrogen). CD45^{high}CD11b^{high} (myeloid cells), CD45^{int} CD11b^{high} (microglia) and CD45^{low} (astrocyte and oligodendrocyte) cells were sorted from the CNS using a BD FACSMelody cell sorter (BD Bioscience) and RNA was extracted using a Quick-RNA Miniprep Kit (Zymo Research, Irvine, CA). cDNA was generated with MMLV reverse transcriptase (Promega, Madison, WI). Real-time PCR was performed using Radiant qPCR mastermix (Alkali Scientific, Fort Lauderdale, FL) or SYBR Green Master Mix (Applied Biosystems, Waltham, MA) in a QuantStudio 3 Real-Time PCR System (Applied Biosystems). Taqman primers used are: *Il1b* (Mm00434228_m1), *Il17a* (Mm00439618_m1), *Rorc* (Mm01261022_m1), *Hif1a* (Mm00468869_m1), *Hk2* (Mm00443385_m1), and *Pdk1* (Mm00554300_m1). All genes were normalized to *Gapdh*. The SYBR primers were listed in Supplementary Table 1.

Flow Cytometry

CNS mononuclear cells were isolated from brain and spinal cord tissues by 70%/30% Percoll density gradient. Surface staining of mononuclear cells was performed with anti-CD4 (RM4–5), anti-CD44 (IM7). anti-CD25 (PC61.5), anti-GITR (DTA-1), anti-ICOS (C398.4A), anti-CD11b (M1/70), anti-CD45 (I3/2.3), anti-MHC Class II (M5/114.15.2),

anti-CD206 (C068C2), anti-Ly6G (1A8), and anti-iNOS (CXNFT) antibodies. For intracellular cytokine detection, cells were stimulated for 4 h with PMA (10ng/mL, Millipore-Sigma) / ionomycin (1μM, Millipore-Sigma) for 4 h in the presence of 2μM monensin (Calbiochem) during the last 2 h of stimulation. Cells were then fixed with 4% paraformaldehyde, washed with PBS, permeabilized with perm buffer, and stained with anti-IL-17A (TC11–18H10), anti-IFNγ (XMG1.2), anti-TNFα (TN3–19), anti-GM-CSF (MP1–22E9) antibodies. All the Abs were purchased from eBioscience (San Diego, CA), BD Biosciences (San Diego, CA) and BioLegend (San Diego, CA). Samples were acquired on a FACSCelesta flow cytometer (BD Biosciences) and analyzed with a FlowJo software (TreeStar, Ashland, OR).

Immunohistochemistry of spinal cord sections

For immunohistochemistry, WT and *Ifit2*$^{-/-}$ mice were perfused intracardially with 4% paraformaldehyde (PFA) under anesthesia. The spinal cord was isolated and post-fixed with 4% PFA overnight and then placed in 30% sucrose at 4°C. After the samples had sunk, the spinal cord was dissected into cervical, thoracic and lumbar tissue blocks, embedded in OCT compound (Scigen-Tissue Plus) and frozen on dry ice. Cryostat sections (10μm) were cut on a Leica cryotome and affixed to Superfrost™ Plus Microscope Slides (FisherScientific). Sections were thawed, air-dried, rehydrated with PBS and further non-specific binding was blocked using 5% goat serum. The following antibodies were incubated in 0.1% Triton with 2% goat serum in PBS at 4°C overnight: rabbit anti-Gfap (1:1000, DAKO, Z0334), rabbit anti-Iba-1 (1:500, Abcam, AB178846), rabbit anti-Tmem119 (1:250, Abcam, ab209064), rat anti-MBP (1:500, Millipore-Sigma, MAB386) and mouse anti-NF200 (1:500, Sigma, N5389) antibodies. Double staining was performed for Mbp and Gfap, or Iba-1 and Tmem119. In addition, to access the amount of myelin debris accumulation in the spinal cord tissues post EAE, rabbit polyclonal antibodies were used against degraded myelin basic protein (dMBP) (1:1000, Millipore-Sigma, AB5864). The sections were then washed in PBS and incubated with a secondary antibody conjugated to Alexa Fluor 488 or Alexa Fluor 555 (1:1000, Invitrogen) for 2 hrs. After washing, slides were mounted with prolong Gold antifade reagent with DAPI (Invitrogen). Images were taken with a Zeiss AX10 (Imager Z2) confocal microscope. MBP-DAB immunohistochemistry was performed using biotinylated secondary antibodies (Vector Laboratories) after primary antibody incubation, overnight at 4°C, biotin–avidin–peroxidase complex (Vector Laboratories) and diaminobenzidine (DAB, Vector Laboratories) were used as the developing agent. Images were taken with a Leica DM 5500B microscope. For quantitation of MBP, dMBP, Iba-1, Tmem119 and GFAP immunostained area, 8 images from randomly selected ROIs/mice were captured. Three mice per condition was used. The images were binarized and the area above threshold was measured using Image J. Average percent area coverage was calculated from all ROIs collected from 3 animals per group using the same imaging and threshold settings. Microglial morphology (n=8 reconstructed microglia/brain) were measured in all mouse brains (n=3/group) by reconstruction and masking tool of IMARIS. The maximum intensity projection of Tmem119^{+} masked images were used to visualize all microglia processes. Binary format images were imported into AnalyzeSkeleton plugin (http://imagejdocu.tudor.lu/) for measuring number of junctions and branches. For the sholl analysis (21), we utilized the line tool to draw a line from the center of each soma to the tip

of its longest process, which provided the length of end radius. The settings of image J sholl analysis plugin were used (start radius-"0.00", step size-2μm, Sholl Method = linear) for the analysis and ramification index was calculated and collected for each cell. Average number of junctions, branches and ramification index was calculated for each group.

Organotypic Slice culture

Organotypic cerebellar slice culture were established from 5 to 8-day-old pups from WT and *Ifit2*$^{-/-}$ mice (n=3/group) according to Tripathi et al. (22). Briefly, brains of P5 to P8 pups were removed and placed in ice-cold artificial cerebral spinal fluid (2 mM calcium chloride, 10 mM glucose, 3 mM potassium chloride, 4 mM magnesium sulphate, 26 mM sodium bicarbonate, 2 mM Ascorbic acid). Excess brain regions were removed, and cerebellum was embedded in 2% low-melting agarose with artificial cerebrospinal fluid. Using Vibratome, 300 μm sagittal slices of the cerebellum were sectioned. Six to seven slices were placed onto cell-culture inserts (Millicell 0.4m, Millipore) in media containing 50% MEM, 25% Horse Serum, 25% Hank's Buffer, 1% GlutaMax, 10 mg/ml Glucose and 1x antibiotic-antimycotic. To study demyelination, slices, after five days in culture, were incubated with 0.5mg/ml lysolecithin for 20h. For remyelination, slices were washed with media (3x) and cultured an additional 6–7 days for remyelination. For immunofluorescence staining, slices were fixed with 4% PFA for 30 min, permeabilized with 2% Triton X-100 for 30 min, and blocked with 10% donkey serum and 0.1% Triton X-100 in PBS for 1 h at room temperature before being incubated in the primary antibodies against neurofilament (mouse anti-NF200, 1:750) and myelin (rat anti-MBP, 1:250) overnight at 4 °C. Primary antibodies were visualized by incubating sections with the appropriate Alexa fluorophore-conjugated secondary antibodies for 1h at room temperature. After mounting the slices, images were taken with a Zeiss AX10 (Imager Z2) confocal microscope. The Image J Plugin JaCoP (23) was used to analyze NF and Mbp co-localization and myelination index. Myelination index describes the fraction of NF and Mbp co-localized area in relation to total NF stained area (24). The myelination index describes the percentage of myelinated axons in relation to all axons. Myelination index was calculated in six slices per brain and average of each brain was used for statistical calculation and graphical representation.

Seahorse Assay

Bone marrow-derived macrophages were used to measure metabolic profiles. Bone marrow cells from wild type of *Ifit2*$^{-/-}$ mice were cultured in complete DMEM supplemented with L-929 culture media. After 6 days of culture, BMDM were harvested and stimulated with 10ng/ml LPS overnight. Extracellular acidification rate (ECAR) was determined using a Seahorse XFe96 Analyzer (Agilent Technologies, CA).

Statistical Analysis

Statistical significance was determined by the Mann-Whitney test and one way ANOVA using a Prism software (GraphPad, San Diego, CA). $p<0.05$ was considered statistically significant.

Results

Ifit expression is elevated during EAE

We first examined *Ifit* mRNA expression in the spinal cord tissues during EAE. C57BL/6 mice were immunized with MOG peptide in CFA followed by pertussis toxin administration to induce EAE. Spinal cord tissues were harvested at disease onset (7 day), peak (day 14), and remission (day 21) phases. Expression of the *Ifit* mRNAs (*Ifit1*, *Ifit2*, and *Ifit3*) was determined by qPCR analysis. The expression pattern closely matched with the disease activity (Fig 1). It was previously reported that endogenous IFN-I production is localized in the target tissues during EAE and that the resulting enhanced IFNAR signaling activity is related to the disease severity (7). Since IFN-I is the primary stimulus inducing Ifit expression (25), increased *Ifit* mRNA expression in EAE is likely induced by IFN signaling elicited from endogenously produced type I IFN. It is interesting to note that low but detectable basal level expression of *Ifit2* mRNA is observed in naïve tissues (Fig 1).

Ifit whole locus mutant mice are highly susceptible to EAE

We previously reported using the Ifit whole locus (IFIT-WL) knockout mice that viral replication is drastically increased in the absence of the Ifit whole locus (19). To investigate if the lack of Ifit family proteins affects autoimmune inflammation, wild type and *Ifit*$^{-/-}$ (IFIT-WL knockout) mice were induced for EAE. The onset and initial progress appeared to be comparable between the groups. However, *Ifit*$^{-/-}$ mice exhibited more severe disease based on the clinical score (Fig 2A). Consistent with the disease severity, the total numbers of CD4 T cells infiltrating the CNS tissue were significantly increased in KO mice, although the proportion was comparable (Fig 2B). Foxp3^{+} regulatory T (Treg) cells accumulated in the inflamed sites are important in resolving inflammation (26). The proportion of CNS infiltrating Treg cells was similar between the groups (data not shown); however, the absolute number of Treg cells was increased in *Ifit*$^{-/-}$ mice (Fig 2B). Surface expression of Treg cell associated markers, such as ICOS, GITR, and CD25, was comparable between the groups (Fig 2C). Therefore, the susceptibility seen in *Ifit*$^{-/-}$ mice may not be attributed to defects in Treg cell recruitment or activation, although we cannot exclude the possibility that Treg cells may be functionally defective without Ifit. CNS accumulation of effector CD4 T cells expressing encephalitogenic cytokines, IL-17, TNFα, GM-CSF, and IFNγ, were markedly increased in both proportions and total numbers (Fig 2D). This was further supported by gene expression level shown in Supplementary Fig 1. None of the *Ifit* mRNA was found in *Ifit*$^{-/-}$ mice, while all three *Ifit* mRNAs were drastically increased in wild type CNS tissues (Supp Fig 1A). Encephalitogenic cytokine mRNA expression was consistent with flow cytometry data. *Il17a*, *Il1b*, *Tnfa*, and *Rorc* mRNA expression was markedly increased in *Ifit*$^{-/-}$ mice compared to those in WT control mice (Supp Fig 1B). Therefore, Ifits appear to play an important immune regulatory role in controlling encephalitogenic inflammatory responses.

Ifit2$^{-/-}$ mice are highly susceptible to EAE

While the canonical functions of the Ifit proteins could be overlapping, there is also evidence that each Ifit could play a distinct role. For example, Ifit2 protects mice from lethal VSV induced neuropathogenesis, while Ifit1 is dispensable in anti-VSV immunity (27). Ifit2

also plays a unique role in protecting mice from coronavirus induced encephalitis by regulating microglial activation and leukocyte migration (16). Therefore, we investigated if Ifit2 plays a role in EAE independent of other Ifit proteins. *Ifit2*$^{-/-}$ mice were induced for EAE. Analogous to what we observed from *Ifit*$^{-/-}$ mice, we found that the disease onset and initial progress were comparable in WT and *Ifit2*$^{-/-}$ mice. However, *Ifit2*$^{-/-}$ mice continued to develop progressive EAE and to display severe disease as in *Ifit*$^{-/-}$ mice (Fig 3A). CD4 T cells infiltrating the CNS tissues were markedly increased in *Ifit2*$^{-/-}$ mice, although the proportions of CD4 T cells seem comparable between the groups (Fig 3B). Proportion of CNS infiltrating Treg cells were similar (data not shown); however, the absolute numbers were elevated in *Ifit2*$^{-/-}$ mice (Fig 3B). Likewise, Treg cell marker expression such as ICOS, GITR, and CD25 remained unchanged (data not shown). We then examined proinflammatory cytokine expression profiles of CNS infiltrating CD4 T cells. As shown in Fig 3C, CD4 T cell expression of inflammatory cytokines was drastically increased in *Ifit2*$^{-/-}$ mice. Consistent with elevated proinflammatory CD4 T cell profiles in the CNS, the expression of key transcription factors for Th1 and Th17 immunity, *Tbx21* and *Rorc*, was similarly increased in *Ifit2*$^{-/-}$ mice (Fig 3D and data not shown). Therefore, Ifit2 alone may play an immune regulatory function to control the development of encephalitogenic immune responses.

Ifit2 deficiency did not affect IFN-I expression in EAE (Fig 3E). In support, other Ifit proteins, *Ifit1* and *Ifit3*, mRNA expression in the CNS tissues of *Ifit2*$^{-/-}$ mice remained comparable to that of wild type mice, strongly suggesting that endogenous IFN-I production is not affected by the absence of Ifit2 (Fig 3E). This result also suggests that the susceptibility of *Ifit2*$^{-/-}$ mice to EAE cannot be attributed to impaired IFN-I or other Ifit expression and that Ifit2 plays a unique role in modulating inflammatory responses.

Severe EAE and increased T cell infiltration in the CNS were further corroborated by enhanced inflammatory chemokine expression. CCL2 and CCL3 production in the CNS tissue critically regulates EAE pathogenesis through recruiting macrophages and dendritic cells (28, 29). Consistent with severe pathogenesis in *Ifit2*$^{-/-}$ mice, we found that *Ccl2* and *Ccl3* mRNA expression particularly in the spinal cord was markedly increased (Fig 3F). CCL7 is an alternative CCR2 ligand potentially involved in EAE pathogenesis (30, 31), and indeed the *Ccl7* expression was also found increased in the *Ifit2*$^{-/-}$ spinal cord (Fig 3F). Overexpression of CXCL1 in astrocytes enhances EAE development by supporting inflammatory cell recruitment (32). Likewise, CXCR3 ligands, CXCL9 and CXCL10 have been implicated in EAE, where the expression is significantly increased in the CNS (33). Consistent with these reports, we found that Ifit2 deficiency markedly increased all those chemokines *Cxcl1*, *Cxcl9*, and *Cxcl10* (Fig 3F).

APC-derived IL-12 family cytokines are especially important in tuning the activation of pathogenic T cells such as Th17 type cells. We found that IL-23p19 subunit expression was dramatically increased in *Ifit2*$^{-/-}$ mice, although IL-12p35 and IL-12p40 subunit expression remained unchanged (Supp Fig 2). IL-27, composed of IL-27p28 and EBI3 subunits and induced by IFN-I signaling, plays an important role in encephalitogenic inflammation (8, 34). While IL-27 could mediate protective roles in EAE pathogenesis, its expression also represents the extent of inflammatory activity. In support, we found elevated expression

of both subunits of IL-27 in *Ifit2*$^{-/-}$ mice (Supp Fig 2 and data not shown). Taken together, these results demonstrate that Ifit2 deficiency displays broad impacts on unleashing inflammatory mediator expression in the CNS tissues, supporting encephalitogenic immune responses.

Altered phenotypes of myeloid cells in the CNS of Ifit2$^{-/-}$ mice

An imbalance between demyelination and remyelination could trigger disease process in EAE or in MS, and clearing myelin debris derived from demyelination is an important homeostatic process promoting remyelination (35). Myeloid cells including monocyte-derived macrophages or microglia are the central cell types mediating myelin debris clearance (35). Macrophages and microglia undergo differentiation into two distinct subsets, proinflammatory and anti-inflammatory phenotype cells, and the anti-inflammatory phenotype cells are particularly involved in tissue repair (36). In case of demyelinating inflammation, it was reported that reparative phenotype microglia remove myelin debris from the lesion, promoting remyelination process (37, 38). We thus compared infiltrating myeloid cells and CNS resident microglial cells. CD45^{high}CD11b^{high} cells were highly abundant in *Ifit2*$^{-/-}$ mice (Fig 4A). Ly6G^{+} neutrophils were excluded from the CD45^{high}CD11b^{high} cells and the resulting infiltrating myeloid cells (MPs) were also greater in *Ifit2*$^{-/-}$ mice (Fig 4B). Their MHCII expression was significantly elevated in *Ifit2*$^{-/-}$ mice. Interestingly, expression of iNOS, a marker for pro-inflammatory subset, was higher in *Ifit2*$^{-/-}$ myeloid cells (Fig 4B). On the other hand, expression of the mannose receptor, CD206, a marker for anti-inflammatory subset, was substantially lower in *Ifit2*$^{-/-}$ cells (Fig 4B). Microglia, tissue resident macrophages in the CNS, have also been implicated in neuroinflammation (39), and are important sources of cytokines and chemokines. They can similarly polarize into proinflammatory or anti-inflammatory phenotype cells (40). In EAE, microglia undergo expansion and proinflammatory subset differentiation (41, 42). In support, we observed greater expansion of microglia population (CD45^{int}CD11b^{high}) in *Ifit2*$^{-/-}$ mice (Fig 4C). Likewise, microglia expression of MHCII molecule was significantly elevated in *Ifit2*$^{-/-}$ mice. Analogous to infiltrating myeloid cells, upregulation of proinflammatory subset marker, iNOS, and downregulation of CD206 was observed (Fig 4C). The number of microglia was not different between wild type and *Ifit2*$^{-/-}$ mice without EAE induction (Supp Fig 3). Of note, basal level MHCII and iNOS expression was slightly lower in *Ifit2*$^{-/-}$ microglia, while CD206 expression was comparable (Supp Fig 3). Therefore, Ifit2 deficiency appears to have significant impact on myeloid cells and microglia activation and polarization, possibly contributing EAE pathogenesis.

Ifit2 deficiency exacerbates demyelination and axonal loss in EAE

We next investigated if Ifit2 deficiency alters demyelination/remyelination processes in EAE. To evaluate demyelination in the areas of WT and *Ifit2*$^{-/-}$ mice spinal cords after EAE induction, we did 3, 3'-diaminobenzidine (DAB) staining for anti-myelin basic protein (Mbp). As seen by MBP staining in the spinal cord sections, EAE generated a notable myelin damage in *Ifit2*$^{-/-}$ relative to WT mice at the peak of disease (Fig 5A, arrows, thoracic region). We next performed double immunostaining with antibodies to Mbp and NF200 to determine the condition of demyelinated axons and found a rather intact myelin ring (green) around the axons (red). Interestingly, we found several Mbp^{+} myelin

sheaths in *Ifit2*$^{-/-}$ mice that were devoid of NF200 labeled axons (Fig 5B arrow in high magnification), implying that axons have been destroyed or damaged and are consequently negative for NF200 antibody. To determine the extent of demyelination, we quantified Mbp immunostained area (%), relative to WT, *Ifit2*$^{-/-}$ mice exhibited a significant (p=0.0001) reduction in percent Mbp stained area (Fig 5C) in the ventral white matter. We also stained the spinal cord sections for degraded MBP (dMBP), which only stains in areas of myelin degradation (43). As shown in Fig 5D, dMBP staining was markedly increased in *Ifit2*$^{-/-}$ thoracic spinal cord, with abundant Iba-1^{+} cells. Quantification of dMBP stained area (Fig 5E) showed significant increase ($p< 0.0001$) in amount of degraded myelin suggesting inefficient myelin debris clearance. These results demonstrate that myelin degradation and axonal loss are significantly greater without Ifit2.

Ifit2 deficiency exacerbates microgliosis, macrophage infiltration and astrocyte activation in EAE

Microglia, macrophages, and astrocytic activation are all required for immune-mediated demyelination. We examined whether the spinal cords of WT and *Ifit2*$^{-/-}$ mice with EAE reveal any differences in macrophage infiltration and/or microglial activation to see if greater microgliosis/macrophage activity was associated with severe EAE-related pathology in *Ifit2*$^{-/-}$ mice. In thoracic region of the WT and *Ifit2*$^{-/-}$ mice spinal cords, we used Iba-1 to label macrophage/microglial cells. The density of Iba-1^{+} cells in the ventral white matter of all regions of the thoracic spinal cord was greater in *Ifit2*$^{-/-}$ than in WT mice (Fig 6A). Moreover, Mbp^{+} myelin debris engulfed by Iba-1^{+} macrophages were more evident in the *Ifit2*$^{-/-}$ tissue sections (Fig 6A, inset). Of note, infection with the neurotrophic coronavirus MHV-RSA59 resulted in decreased microglial activation and infiltration of peripheral immune cells (NK, CD4 T cells) into the brain in *Ifit2*$^{-/-}$ mice (44), suggesting a unique mode of pathogenesis of EAE in the absence of Ifit2. Several factors may account for the different immune responses of *Ifit2*$^{-/-}$ mice in the model of MHV infection vs. EAE. Different innate immune components (viral RNA and proteins vs. CFA), or alternatively, different route of injection (MHV intrathecal infection vs. subcutaneous CFA immunization) may play a role in eliciting different immune responses. Microglia and peripheral macrophages have different origins, and microglia are activated prior to peripheral immune infiltration and actively assist in their recruitment, which may also be true in EAE. We stained the spinal cord sections for transmembrane protein 119 (Tmem119), which has emerged as a microglia-specific marker, to assess the alteration in microglial numbers. At the peak of disease, quantitation of Tmem119 staining revealed that *Ifit2*$^{-/-}$ mice spinal cord had a significantly (p=0.0018) greater Tmem119^{+} area (%) than WT mice (Fig 6B), supporting the flow cytometry data shown in Fig 4C. Furthermore, Tmem119^{+} microglia in *Ifit2*$^{-/-}$ mice have active phenotypes with amoeboid morphology and retracted microglial processes. Skeletal and sholl analysis confirmed ramified microglial morphology (Fig 6D), with significant reduction in microglial branches (P=0.0009) (Fig 6F), junctions (p=0.0009) (Fig 6E) and ramification index (0.0007) in *Ifit2*$^{-/-}$ mice (Fig 6G). Several reports have demonstrated that astrocytes regulate CNS inflammation by affecting infiltration of peripheral immune cells and activation of resident microglia (45, 46). We thus determined astrocyte activation by immunohistochemistry using antibody against GFAP. We observed that *Ifit2*$^{-/-}$ mice exhibited significantly (p=0.0021) higher GFAP^{+} astrocytes

compared to WT at the peak of EAE (Fig 6C). The degree of astrocyte reactivity is positively correlated with GFAP expression (47, 48), indicating more astrocyte activation in *Ifit2*$^{-/-}$ mice.

Greater demyelination, lack of myelin debris clearance, and loss of remyelination in Ifit2$^{-/-}$ tissues

Anti-inflammatory type microglia and macrophages support CNS remyelination (37). Since both infiltrating myeloid cells and microglia expressing CD206 were diminished in *Ifit2*$^{-/-}$ mice, we sought to test if such defects in anti-inflammatory phenotype differentiation are associated with impaired remyelination and with severe pathogenesis seen in *Ifit2*$^{-/-}$ mice. We chose the model of organotypic slice cultures and lysolecithin (LPC, 0.5mg/ml) induced demyelination and remyelination in P10 WT and *Ifit2*$^{-/-}$ brains (Fig 7A) (22, 49). Slices stained for myelin protein Mbp and axonal marker NF200 in three conditions, namely, control (CT), demyelinated (DM) and remyelinated (RM) (Fig 7B). To investigate the difference in extent of myelination between WT and *Ifit2*$^{-/-}$ slices, we performed the quantification of myelination indices. The control slices (B.I, WT-CT and B.II, *Ifit2*$^{-/-}$-CT) that had not been exposed to LPC showed a comparable myelination index (P=0.99) while upon LPC application there was a strikingly pronounced and significant demyelination (p=0.049) in the *Ifit2*$^{-/-}$ slices (B.IV, *Ifit2*$^{-/-}$- DM) compared to WT (B.III, WT- DM) (Fig 7B). Of particular interest was the lack of myelin debris clearance in the *Ifit2*$^{-/-}$ slices following demyelination (B.IV; shown by the white arrows). We next examined the extent of remyelination as the lack of myelin clearance by microglia and/or macrophages could have negative impact on remyelination (35). Indeed, spontaneous remyelination was observed in WT brain slices (B.V; WT-RM), while remyelination was severely and significantly (p=0.0004) impaired in *Ifit2*$^{-/-}$ brains (B.VI; quantified in 7C; *Ifit2*$^{-/-}$-RM). Of note, based on NF200 staining, we did not see significant difference in axonal loss between the groups, suggesting that defects in remyelination of *Ifit2*$^{-/-}$ brains is not due to loss of axons. As the overall number of OL lineage cells were also comparable in WT and *Ifit2*$^{-/-}$ mouse brains (data not shown), defective remyelination appears to be attributed to impaired myelin debris clearance.

Ifit2 deficiency results in metabolic dysregulation of myeloid cells

Altered differentiation profiles of infiltrating myeloid cells and of microglia (Fig 4), exacerbated demyelination (Fig 5 and 6), and defects in myelin debris clearance and remyelination (Fig 7) observed in *Ifit2*$^{-/-}$ CNS tissues prompted us to investigate whether Ifit2 deficiency dysregulates metabolic profiles of those myeloid cells. Proinflammatory phenotype cells predominantly utilize glycolysis as an energy source, whereas anti-inflammatory reparative phenotype cells preferentially utilize oxidative phosphorylation (50, 51). We thus measured proinflammatory and metabolic gene expression in WT and *Ifit2*$^{-/-}$ bone marrow derived macrophages (BMDM) following stimulation with LPS and IL-4 to trigger proinflammatory and anti-inflammatory phenotype cell differentiation, respectively. We found that *Ifit2*$^{-/-}$ BMDM expressed higher proinflammatory cytokines, *Tnfa* and *Il1b*, following LPS stimulation. In addition, glycolytic gene, hypoxia-inducible transcription factor (*Hif1a*) and hexokinase 2 (*Hk2*) expression was also elevated in *Ifit2*$^{-/-}$ BMDM cells following LPS stimulation (Fig 8A). IL-4 stimulation, which promotes anti-inflammatory

macrophage differentiation (52), also enhanced *Il1b* and *Hif1a* expression in *Ifit2*$^{-/-}$ BMDM cells (Fig 8A). We then examined expression of genes involved in glycolysis from CNS tissues of EAE induced mice. We measured the *Hk2*, pyruvate dehydrogenase kinase 1 (*pdk1*), and *Hif1a*, all of which play a critical role in glycolysis (53–55). The gene expression was drastically increased in the CNS tissues of *Ifit2*$^{-/-}$ mice (Fig 8B). Therefore, Ifit2 deficiency appears to be associated with dysregulated inflammatory cytokine and metabolic gene expression in vivo.

To further investigate Ifit2-dependent metabolic profiles in myeloid cells and in microglia of mice with ongoing EAE, we isolated infiltrating myeloid cells (CD45^{high} CD11b^{high}), microglia (CD45^{int} CD11b^{high}), and CD45^{low} cells (including oligodendrocytes and astrocytes) from wild type and *Ifit2*$^{-/-}$ mice induced for EAE. Expression of *Hk2*, *Pdk1*, and *Hif1a* was significantly enhanced in these cells of *Ifit2*$^{-/-}$ mice compared to those of WT mice (Fig 8C). Moreover, extracellular acidification rate (ECAR) of *Ifit2*$^{-/-}$ BMDM was substantially greater than WT cells when stimulated with LPS (Fig 8D). These results strongly suggest that Ifit2 appears to control metabolic programming of myeloid cells in vivo. Such altered metabolic programming in *Ifit2*$^{-/-}$ mice may result in preferential proinflammatory subset differentiation, which then have direct impact on disease progression, particularly remyelination process through myelin debris clearance.

Discussion

In the present study, we report an unexpected role for Ifit2, one of type I IFN-induced gene products known for potent anti-viral functions, in modulating autoimmune inflammation. Mice deficient in Ifit2 were highly susceptible to myelin antigen-reactive autoimmunity, EAE. The susceptibility was closely associated with heightened encephalitogenic T cell responses with elevated proinflammatory cytokine production. Also found was enhanced expression of chemokines supporting inflammatory cell recruitment to the target tissues. Importantly, we noticed that Ifit2 deficiency resulted in severe demyelination and impaired remyelination processes, which appear to contribute to the exacerbated disease. Myelin debris clearance predominantly mediated by reparative macrophage and microglia subset is known to play a key role in remyelination. One notable feature of proinflammatory and tissue repair subsets of myeloid cells is their metabolic profiles, i.e., glycolytic pathways in proinflammatory phenotype cells vs. oxidative phosphorylation in reparative phenotype cells. Indeed, we found that, in *Ifit2*$^{-/-}$ infiltrating myeloid and CNS resident microglia, expression of genes involved in glycolytic pathways as well as extracellular acidification rate measured by Seahorse XF analyzer was markedly increased. Therefore, our results demonstrate that Ifit2 may play a novel regulatory function limiting inflammatory responses by balancing metabolic profiles and differentiation process of myeloid lineage cells.

To our knowledge, the present study reports for the first time that Ifit2 expresses an immune regulatory function in autoimmunity. In EAE, all three IFIT family proteins (Ifit1, Ifit2, and Ifit3) are strongly induced especially in the CNS tissues, and the kinetics of the expression closely mirrors the disease activity. Given that endogenous IFN-I production in EAE is predominantly found in the target tissues (7), the IFN-I may be responsible for the Ifits expressed within the CNS. The entire *Ifit* locus knockout animals display exacerbated

disease, and we found that Ifit2 deficiency alone is sufficient for similar susceptibility to EAE. Therefore, Ifit2's ability to regulate autoimmune inflammation may be unique to IFIT2 protein. It is important to point out that the *Ifna*, *Ifnb*, *Ifit1*, and *Ifit3* mRNA expression in *Ifit2*$^{-/-}$ mice remain intact, indicating that high susceptibility of *Ifit2*$^{-/-}$ mice to EAE is not attributable to defective IFN-I signaling or other IFIT production.

Mice deficient in type I IFN receptor (IFNAR) are highly susceptible to EAE (7). Thus, IFN-I stimulation and subsequent Ifit2 induction could be crucial in limiting inflammatory responses. Likewise, the lack of TRIF, an adaptor molecule necessary to induce IFN-I production, also results in exacerbated EAE (8). The precise upstream signal that activates TRIF to induce IFN-I production within the CNS remains to be determined. Protective functions of TRIF suggest that ligands activating TLR3 or TLR4 may be involved in inducing IFN-I production in EAE. In support, TLR3 stimulation was previously shown to suppress EAE (56). Moreover, neonatal exposure to LPS can suppress EAE by inducing tolerogenic dendritic cells (57). However, pretreatment of LPS only prior to EAE induction is known to delay onset of the disease, while the severity remains unchanged (58). Paradoxically, mice deficient in the *Tlr4* gene surprisingly develop more severe EAE, suggesting the pathogenic role (59). Alarmin S100A9 is an alternative ligand for TLR4 (60), and S100A9-deficient mice were previously shown to develop exacerbated EAE (61). It will be important to identify endogenous signals activating the TRIF-IFN-I-IFIT signaling pathways in EAE pathogenesis. However, Ifit expression may also be triggered independently of IFN-I, especially through signals generated via pattern recognition receptors (PRR) or RNA sensors like MDA5 and RIG-I (12). Thus, future investigation should focus on identifying the precise signals responsible for Ifit induction in EAE.

Cell type specific *Ifnar*-deficient mouse models were previously used to determine the target cells responsible for the severe EAE seen in *Ifnar*$^{-/-}$ mice (7). T cell- or neuron-expression of IFNAR is found dispensable, whereas targeting IFNAR in myeloid lineage cells phenocopies global IFNAR deficiency, suggesting that infiltrating inflammatory monocytes as well as CNS resident microglia may likely be the target cells of IFN-I (7). Therefore, we speculate that myeloid lineage cells are likely the source of Ifit2-expressing cells. The exact mechanisms by which IFN-I is endogenously produced (i.e., via TRIF-dependent mechanism) and acts on the target cells (i.e., via IFNAR-IFIT2-dependent mechanism) to mediate protective roles are areas of our current investigation.

It is interesting to note that Ifit2 deficiency is closely associated with severe demyelination and defective remyelination. Following demyelination, macrophages and microglia play a crucial role in clearing myelin debris, which is known to be instrumental to support the subsequent remyelination to occur (35). Ifit2-deficient spinal cord tissues displayed greater degraded MBP expression along with increased accumulation of infiltrating Iba-1^{+} myeloid cells, microglia, and astrocytes. Our recent report similarly identified a unique function of Ifit2 that protects the host from lethal neurotropic MHV infection by modulating microglia activation and recruitment (16). Unlike the present study where CNS infiltrating myeloid cells and microglia are abundant in *Ifit2*$^{-/-}$ mice with EAE, Ifit2 deficiency results in impaired microglial activation as well as reduced infiltration of inflammatory cells (16). Mechanism underlying the opposite effects of Ifit2 remains to be investigated.

Innate immune responses induced by virus infection vs. autoimmune inflammation may be responsible for the difference.

From the LPC-induced demyelination/remyelination organotypic slice culture and immunofluorescence microscopic examination experiments, we observed that Ifit2 deficiency is also associated with defective myelin debris clearance and remyelination processes. Importantly, myelin debris clearance is one key property of anti-inflammatory phenotype macrophage/microglia (35). Therefore, it is possible that Ifit2 deficiency may impair transition from proinflammatory to anti-inflammatory phenotype cell differentiation, which occurs during EAE (37, 62). Pro- and anti-inflammatory phenotype macrophages (and microglia) utilize different metabolic programs, glycolysis and oxidative phosphorylation, respectively. Indeed, we noticed drastically elevated glycolytic gene expression as well as extracellular acidification rate representing glycolysis in *Ifit2*$^{-/-}$ BMDM. In addition, *Ifit2*$^{-/-}$ BMDM expression of proinflammatory cytokines, especially IL-1β, was markedly increased compared to wild type cells, even after IL-4 stimulation, which is known to promote anti-inflammatory subset differentiation (52). Consistent with this, IFN-I promotes fatty acid oxidation and oxidative phosphorylation (63). Supporting the possibilities, expression of key glycolytic genes in CNS infiltrating myeloid cells and microglia in *Ifit2*$^{-/-}$ mice with EAE was found drastically elevated. Therefore, we would argue that Ifit2 may be an important metabolic switch that balances metabolism of macrophages (and microglia) to trigger remyelinating tissue repair processes by supporting anti-inflammatory subset differentiation. IFN-I is a widely used therapeutic option in MS patients. However, there is a cohort of patient refractory to the treatment (64). Paradoxically, IFN-I could play a pathogenic role in other autoimmune conditions such as Lupus (65). Better defining the precise cellular and molecular mechanisms will be a subject of great importance to identify novel therapeutic approaches for both IFN-I-responsive and -refractory inflammatory conditions, including but not limited to, MS.

Supplementary Material

Refer to Web version on PubMed Central for supplementary material.

Acknowledgements

The authors thank support by the Northwestern University Interdepartmental ImmunoBiology Flow Cytometry Core Facility, and members of the Min, Sen, and Dutta laboratories for helpful discussion.

Supported by:

NIH grants AI125247, NS123532 and CA068782.

Bibliography

1. Benveniste EN, and Qin H. 2007. Type I interferons as anti-inflammatory mediators. Sci STKE 2007: pe70.
2. Chen K, Liu J, and Cao X. 2017. Regulation of type I interferon signaling in immunity and inflammation: A comprehensive review. J Autoimmun 83: 1–11. [PubMed: 28330758]
3. Sormani MP, and De Stefano N. 2013. Defining and scoring response to IFN-beta in multiple sclerosis. Nat Rev Neurol 9: 504–512. [PubMed: 23897407]

4. Filippini G, Munari L, Incorvaia B, Ebers GC, Polman C, D'Amico R, and Rice GP. 2003. Interferons in relapsing remitting multiple sclerosis: a systematic review. Lancet 361: 545–552. [PubMed: 12598138]
5. Inoue M, Williams KL, Oliver T, Vandenabeele P, Rajan JV, Miao EA, and Shinohara ML. 2012. Interferon-beta therapy against EAE is effective only when development of the disease depends on the NLRP3 inflammasome. Sci Signal 5: ra38.
6. Shinohara ML, Kim JH, Garcia VA, and Cantor H. 2008. Engagement of the type I interferon receptor on dendritic cells inhibits T helper 17 cell development: role of intracellular osteopontin. Immunity 29: 68–78. [PubMed: 18619869]
7. Prinz M, Schmidt H, Mildner A, Knobeloch KP, Hanisch UK, Raasch J, Merkler D, Detje C, Gutcher I, Mages J, Lang R, Martin R, Gold R, Becher B, Bruck W, and Kalinke U. 2008. Distinct and nonredundant in vivo functions of IFNAR on myeloid cells limit autoimmunity in the central nervous system. Immunity 28: 675–686. [PubMed: 18424188]
8. Guo B, Chang EY, and Cheng G. 2008. The type I IFN induction pathway constrains Th17-mediated autoimmune inflammation in mice. J Clin Invest 118: 1680–1690. [PubMed: 18382764]
9. Lee AJ, and Ashkar AA. 2018. The Dual Nature of Type I and Type II Interferons. Front Immunol 9: 2061. [PubMed: 30254639]
10. McNab F, Mayer-Barber K, Sher A, Wack A, and O'Garra A. 2015. Type I interferons in infectious disease. Nat Rev Immunol 15: 87–103. [PubMed: 25614319]
11. Pidugu VK, Pidugu HB, Wu MM, Liu CJ, and Lee TC. 2019. Emerging Functions of Human IFIT Proteins in Cancer. Front Mol Biosci 6: 148. [PubMed: 31921891]
12. Diamond MS, and Farzan M. 2013. The broad-spectrum antiviral functions of IFIT and IFITM proteins. Nat Rev Immunol 13: 46–57. [PubMed: 23237964]
13. Johnson B, VanBlargan LA, Xu W, White JP, Shan C, Shi PY, Zhang R, Adhikari J, Gross ML, Leung DW, Diamond MS, and Amarasinghe GK. 2018. Human IFIT3 Modulates IFIT1 RNA Binding Specificity and Protein Stability. Immunity 48: 487–499 e485. [PubMed: 29525521]
14. Pichlmair A, Lassnig C, Eberle CA, Gorna MW, Baumann CL, Burkard TR, Burckstummer T, Stefanovic A, Krieger S, Bennett KL, Rulicke T, Weber F, Colinge J, Muller M, and Superti-Furga G. 2011. IFIT1 is an antiviral protein that recognizes 5'-triphosphate RNA. Nat Immunol 12: 624–630. [PubMed: 21642987]
15. Yang Z, Liang H, Zhou Q, Li Y, Chen H, Ye W, Chen D, Fleming J, Shu H, and Liu Y. 2012. Crystal structure of ISG54 reveals a novel RNA binding structure and potential functional mechanisms. Cell Res 22: 1328–1338. [PubMed: 22825553]
16. Das Sarma J, Burrows A, Rayman P, Hwang MH, Kundu S, Sharma N, Bergmann C, and Sen GC. 2020. Ifit2 deficiency restricts microglial activation and leukocyte migration following murine coronavirus (m-CoV) CNS infection. PLoS Pathog 16: e1009034.
17. John SP, Sun J, Carlson RJ, Cao B, Bradfield CJ, Song J, Smelkinson M, and Fraser IDC. 2018. IFIT1 Exerts Opposing Regulatory Effects on the Inflammatory and Interferon Gene Programs in LPS-Activated Human Macrophages. Cell Rep 25: 95–106 e106. [PubMed: 30282041]
18. Imaizumi T, Sassa N, Kawaguchi S, Matsumiya T, Yoshida H, Seya K, Shiratori T, Hirono K, and Tanaka H. 2018. Interferon-stimulated gene 60 (ISG60) constitutes a negative feedback loop in the downstream of TLR3 signaling in hCMEC/D3 cells. J Neuroimmunol 324: 16–21. [PubMed: 30195920]
19. Kimura T, Flynn CT, Alirezaei M, Sen GC, and Whitton JL. 2019. Biphasic and cardiomyocyte-specific IFIT activity protects cardiomyocytes from enteroviral infection. PLoS Pathog 15: e1007674. [PubMed: 30958867]
20. Butchi NB, Hinton DR, Stohlman SA, Kapil P, Fensterl V, Sen GC, and Bergmann CC. 2014. Ifit2 deficiency results in uncontrolled neurotropic coronavirus replication and enhanced encephalitis via impaired alpha/beta interferon induction in macrophages. J Virol 88: 1051–1064. [PubMed: 24198415]
21. Ferreira TA, Blackman AV, Oyrer J, Jayabal S, Chung AJ, Watt AJ, Sjostrom PJ, and van Meyel DJ. 2014. Neuronal morphometry directly from bitmap images. Nat Methods 11: 982–984. [PubMed: 25264773]

22. Tripathi A, Volsko C, Garcia JP, Agirre E, Allan KC, Tesar PJ, Trapp BD, Castelo-Branco G, Sim FJ, and Dutta R. 2019. Oligodendrocyte Intrinsic miR-27a Controls Myelination and Remyelination. Cell Rep 29: 904–919 e909. [PubMed: 31644912]
23. Bolte S, and Cordelieres FP. 2006. A guided tour into subcellular colocalization analysis in light microscopy. J Microsc 224: 213–232. [PubMed: 17210054]
24. Bauch J, Ort SV, Ulc A, and Faissner A. 2022. Tenascins Interfere With Remyelination in an Ex Vivo Cerebellar Explant Model of Demyelination. Front Cell Dev Biol 10: 819967.
25. Zhou X, Michal JJ, Zhang L, Ding B, Lunney JK, Liu B, and Jiang Z. 2013. Interferon induced IFIT family genes in host antiviral defense. Int J Biol Sci 9: 200–208. [PubMed: 23459883]
26. Gilroy D, and De Maeyer R. 2015. New insights into the resolution of inflammation. Semin Immunol 27: 161–168. [PubMed: 26037968]
27. Fensterl V, Wetzel JL, Ramachandran S, Ogino T, Stohlman SA, Bergmann CC, Diamond MS, Virgin HW, and Sen GC. 2012. Interferon-induced Ifit2/ISG54 protects mice from lethal VSV neuropathogenesis. PLoS Pathog 8: e1002712. [PubMed: 22615570]
28. Dogan RN, Elhofy A, and Karpus WJ. 2008. Production of CCL2 by central nervous system cells regulates development of murine experimental autoimmune encephalomyelitis through the recruitment of TNF- and iNOS-expressing macrophages and myeloid dendritic cells. J Immunol 180: 7376–7384. [PubMed: 18490737]
29. Manczak M, Jiang S, Orzechowska B, and Adamus G. 2002. Crucial role of CCL3/MIP-1alpha in the recurrence of autoimmune anterior uveitis induced with myelin basic protein in Lewis rats. J Autoimmun 18: 259–270. [PubMed: 12144807]
30. Mildner A, Mack M, Schmidt H, Bruck W, Djukic M, Zabel MD, Hille A, Priller J, and Prinz M. 2009. CCR2+Ly-6Chi monocytes are crucial for the effector phase of autoimmunity in the central nervous system. Brain 132: 2487–2500. [PubMed: 19531531]
31. Zhang Y, Han JJ, Liang XY, Zhao L, Zhang F, Rasouli J, Wang ZZ, Zhang GX, and Li X. 2018. miR-23b Suppresses Leukocyte Migration and Pathogenesis of Experimental Autoimmune Encephalomyelitis by Targeting CCL7. Mol Ther 26: 582–592. [PubMed: 29275848]
32. Grist JJ, Marro BS, Skinner DD, Syage AR, Worne C, Doty DJ, Fujinami RS, and Lane TE. 2018. Induced CNS expression of CXCL1 augments neurologic disease in a murine model of multiple sclerosis via enhanced neutrophil recruitment. Eur J Immunol 48: 1199–1210. [PubMed: 29697856]
33. Carter SL, Muller M, Manders PM, and Campbell IL. 2007. Induction of the genes for Cxcl9 and Cxcl10 is dependent on IFN-gamma but shows differential cellular expression in experimental autoimmune encephalomyelitis and by astrocytes and microglia in vitro. Glia 55: 1728–1739. [PubMed: 17902170]
34. Fitzgerald DC, Ciric B, Touil T, Harle H, Grammatikopolou J, Das Sarma J, Gran B, Zhang GX, and Rostami A. 2007. Suppressive effect of IL-27 on encephalitogenic Th17 cells and the effector phase of experimental autoimmune encephalomyelitis. J Immunol 179: 3268–3275. [PubMed: 17709543]
35. Lampron A, Larochelle A, Laflamme N, Prefontaine P, Plante MM, Sanchez MG, Yong VW, Stys PK, Tremblay ME, and Rivest S. 2015. Inefficient clearance of myelin debris by microglia impairs remyelinating processes. J Exp Med 212: 481–495. [PubMed: 25779633]
36. Das A, Sinha M, Datta S, Abas M, Chaffee S, Sen CK, and Roy S. 2015. Monocyte and macrophage plasticity in tissue repair and regeneration. Am J Pathol 185: 2596–2606. [PubMed: 26118749]
37. Miron VE, Boyd A, Zhao JW, Yuen TJ, Ruckh JM, Shadrach JL, van Wijngaarden P, Wagers AJ, Williams A, Franklin RJM, and Ffrench-Constant C. 2013. M2 microglia and macrophages drive oligodendrocyte differentiation during CNS remyelination. Nat Neurosci 16: 1211–1218. [PubMed: 23872599]
38. Lloyd AF, and Miron VE. 2019. The pro-remyelination properties of microglia in the central nervous system. Nat Rev Neurol 15: 447–458. [PubMed: 31256193]
39. Goldmann T, and Prinz M. 2013. Role of microglia in CNS autoimmunity. Clin Dev Immunol 2013: 208093.

40. Orihuela R, McPherson CA, and Harry GJ. 2016. Microglial M1/M2 polarization and metabolic states. Br J Pharmacol 173: 649–665. [PubMed: 25800044]
41. Tay TL, Mai D, Dautzenberg J, Fernandez-Klett F, Lin G, Sagar, Datta M, Drougard A, Stempfl T, Ardura-Fabregat A, Staszewski O, Margineanu A, Sporbert A, Steinmetz LM, Pospisilik JA, Jung S, Priller J, Grun D, Ronneberger O, and Prinz M. 2017. A new fate mapping system reveals context-dependent random or clonal expansion of microglia. Nat Neurosci 20: 793–803. [PubMed: 28414331]
42. Prajeeth CK, Lohr K, Floess S, Zimmermann J, Ulrich R, Gudi V, Beineke A, Baumgartner W, Muller M, Huehn J, and Stangel M. 2014. Effector molecules released by Th1 but not Th17 cells drive an M1 response in microglia. Brain Behav Immun 37: 248–259. [PubMed: 24412213]
43. Matsuo A, Lee GC, Terai K, Takami K, Hickey WF, McGeer EG, and McGeer PL. 1997. Unmasking of an unusual myelin basic protein epitope during the process of myelin degeneration in humans: a potential mechanism for the generation of autoantigens. Am J Pathol 150: 1253–1266. [PubMed: 9094982]
44. Saadi F, Chakravarty D, Kumar S, Kamble M, Saha B, Shindler KS, and Das Sarma J. 2021. CD40L protects against mouse hepatitis virus-induced neuroinflammatory demyelination. PLoS Pathog 17: e1010059. [PubMed: 34898656]
45. Ransohoff RM, Hamilton TA, Tani M, Stoler MH, Shick HE, Major JA, Estes ML, Thomas DM, and Tuohy VK. 1993. Astrocyte expression of mRNA encoding cytokines IP-10 and JE/MCP-1 in experimental autoimmune encephalomyelitis. FASEB J 7: 592–600. [PubMed: 8472896]
46. Brambilla R, Morton PD, Ashbaugh JJ, Karmally S, Lambertsen KL, and Bethea JR. 2014. Astrocytes play a key role in EAE pathophysiology by orchestrating in the CNS the inflammatory response of resident and peripheral immune cells and by suppressing remyelination. Glia 62: 452–467. [PubMed: 24357067]
47. Sofroniew MV 2009. Molecular dissection of reactive astrogliosis and glial scar formation. Trends Neurosci 32: 638–647. [PubMed: 19782411]
48. Anderson MA, Ao Y, and Sofroniew MV. 2014. Heterogeneity of reactive astrocytes. Neurosci Lett 565: 23–29. [PubMed: 24361547]
49. Dutta R, Chomyk AM, Chang A, Ribaudo MV, Deckard SA, Doud MK, Edberg DD, Bai B, Li M, Baranzini SE, Fox RJ, Staugaitis SM, Macklin WB, and Trapp BD. 2013. Hippocampal demyelination and memory dysfunction are associated with increased levels of the neuronal microRNA miR-124 and reduced AMPA receptors. Ann Neurol 73: 637–645. [PubMed: 23595422]
50. Viola A, Munari F, Sanchez-Rodriguez R, Scolaro T, and Castegna A. 2019. The Metabolic Signature of Macrophage Responses. Front Immunol 10: 1462. [PubMed: 31333642]
51. Wang F, Zhang S, Vuckovic I, Jeon R, Lerman A, Folmes CD, Dzeja PP, and Herrmann J. 2018. Glycolytic Stimulation Is Not a Requirement for M2 Macrophage Differentiation. Cell Metab 28: 463–475 e464. [PubMed: 30184486]
52. Hu X, Leak RK, Shi Y, Suenaga J, Gao Y, Zheng P, and Chen J. 2015. Microglial and macrophage polarization-new prospects for brain repair. Nat Rev Neurol 11: 56–64. [PubMed: 25385337]
53. Wolf A, Agnihotri S, Micallef J, Mukherjee J, Sabha N, Cairns R, Hawkins C, and Guha A. 2011. Hexokinase 2 is a key mediator of aerobic glycolysis and promotes tumor growth in human glioblastoma multiforme. J Exp Med 208: 313–326. [PubMed: 21242296]
54. Dupuy F, Tabaries S, Andrzejewski S, Dong Z, Blagih J, Annis MG, Omeroglu A, Gao D, Leung S, Amir E, Clemons M, Aguilar-Mahecha A, Basik M, Vincent EE, St-Pierre J, Jones RG, and Siegel PM. 2015. PDK1-Dependent Metabolic Reprogramming Dictates Metastatic Potential in Breast Cancer. Cell Metab 22: 577–589. [PubMed: 26365179]
55. Lum JJ, Bui T, Gruber M, Gordan JD, DeBerardinis RJ, Covello KL, Simon MC, and Thompson CB. 2007. The transcription factor HIF-1alpha plays a critical role in the growth factor-dependent regulation of both aerobic and anaerobic glycolysis. Genes Dev 21: 1037–1049. [PubMed: 17437992]
56. Touil T, Fitzgerald D, Zhang GX, Rostami A, and Gran B. 2006. Cutting Edge: TLR3 stimulation suppresses experimental autoimmune encephalomyelitis by inducing endogenous IFN-beta. J Immunol 177: 7505–7509. [PubMed: 17114417]

57. Ellestad KK, Tsutsui S, Noorbakhsh F, Warren KG, Yong VW, Pittman QJ, and Power C. 2009. Early life exposure to lipopolysaccharide suppresses experimental autoimmune encephalomyelitis by promoting tolerogenic dendritic cells and regulatory T cells. J Immunol 183: 298–309. [PubMed: 19542441]

58. Buenafe AC, and Bourdette DN. 2007. Lipopolysaccharide pretreatment modulates the disease course in experimental autoimmune encephalomyelitis. J Neuroimmunol 182: 32–40. [PubMed: 17055066]

59. Marta M, Andersson A, Isaksson M, Kampe O, and Lobell A. 2008. Unexpected regulatory roles of TLR4 and TLR9 in experimental autoimmune encephalomyelitis. Eur J Immunol 38: 565–575. [PubMed: 18203139]

60. He Z, Riva M, Bjork P, Sward K, Morgelin M, Leanderson T, and Ivars F. 2016. CD14 Is a Co-Receptor for TLR4 in the S100A9-Induced Pro-Inflammatory Response in Monocytes. PLoS One 11: e0156377.

61. Bjork P, Bjork A, Vogl T, Stenstrom M, Liberg D, Olsson A, Roth J, Ivars F, and Leanderson T. 2009. Identification of human S100A9 as a novel target for treatment of autoimmune disease via binding to quinoline-3-carboxamides. PLoS Biol 7: e97. [PubMed: 19402754]

62. Liu C, Li Y, Yu J, Feng L, Hou S, Liu Y, Guo M, Xie Y, Meng J, Zhang H, Xiao B, and Ma C. 2013. Targeting the shift from M1 to M2 macrophages in experimental autoimmune encephalomyelitis mice treated with fasudil. PLoS One 8: e54841.

63. Wu D, Sanin DE, Everts B, Chen Q, Qiu J, Buck MD, Patterson A, Smith AM, Chang CH, Liu Z, Artyomov MN, Pearce EL, Cella M, and Pearce EJ. 2016. Type 1 Interferons Induce Changes in Core Metabolism that Are Critical for Immune Function. Immunity 44: 1325–1336. [PubMed: 27332732]

64. Sriram U, Barcellos LF, Villoslada P, Rio J, Baranzini SE, Caillier S, Stillman A, Hauser SL, Montalban X, and Oksenberg JR. 2003. Pharmacogenomic analysis of interferon receptor polymorphisms in multiple sclerosis. Genes Immun 4: 147–152. [PubMed: 12618863]

65. Crow MK 2014. Type I interferon in the pathogenesis of lupus. J Immunol 192: 5459–5468. [PubMed: 24907379]

Key points

- Ifit2 deficiency confers susceptibility to autoimmune inflammation.
- Ifit2 deficiency impairs myelin debris clearance and remyelination.
- Metabolic profiles of myeloid cells and microglia are altered without Ifit2.

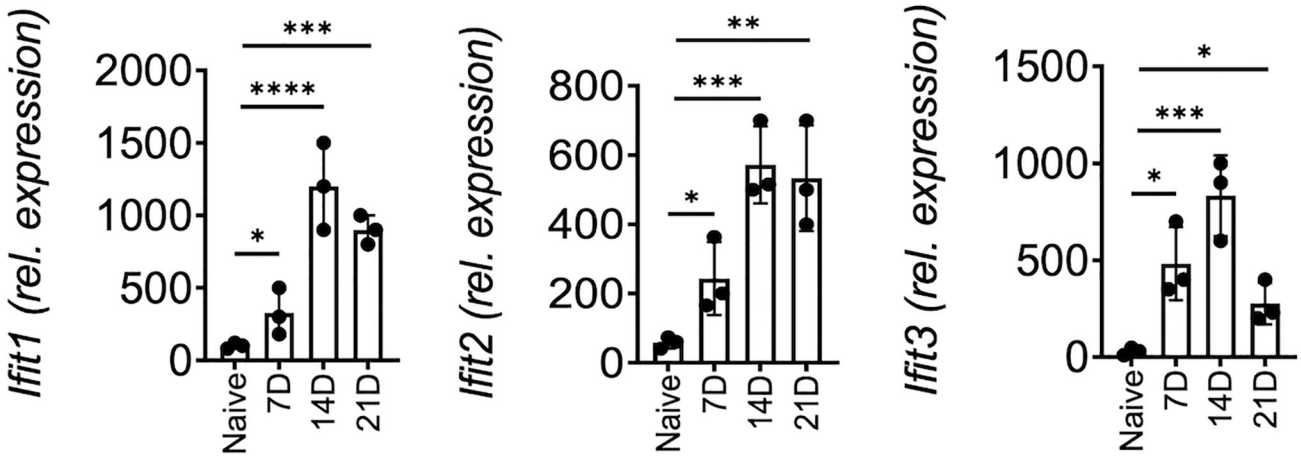

Fig 1. Expression of *Ifit* mRNA in the CNS during EAE.

C57BL/6 mice were injected with CFA/$MOG_{35–55}$ followed by pertussis toxin on the day of immunization and 48 h later to induce EAE. qPCR from whole spinal cord were harvested at disease onset (7 day), peak (day 14), and remission (day 21) phases. Data were normalized to naive mice. The results shown are the mean ± SD of individually tested mice from two independent experiments. *$p < 0.05$; **$p < 0.01$; ***, $p<0.001$; as determined by Mann-Whitney nonparametric test.

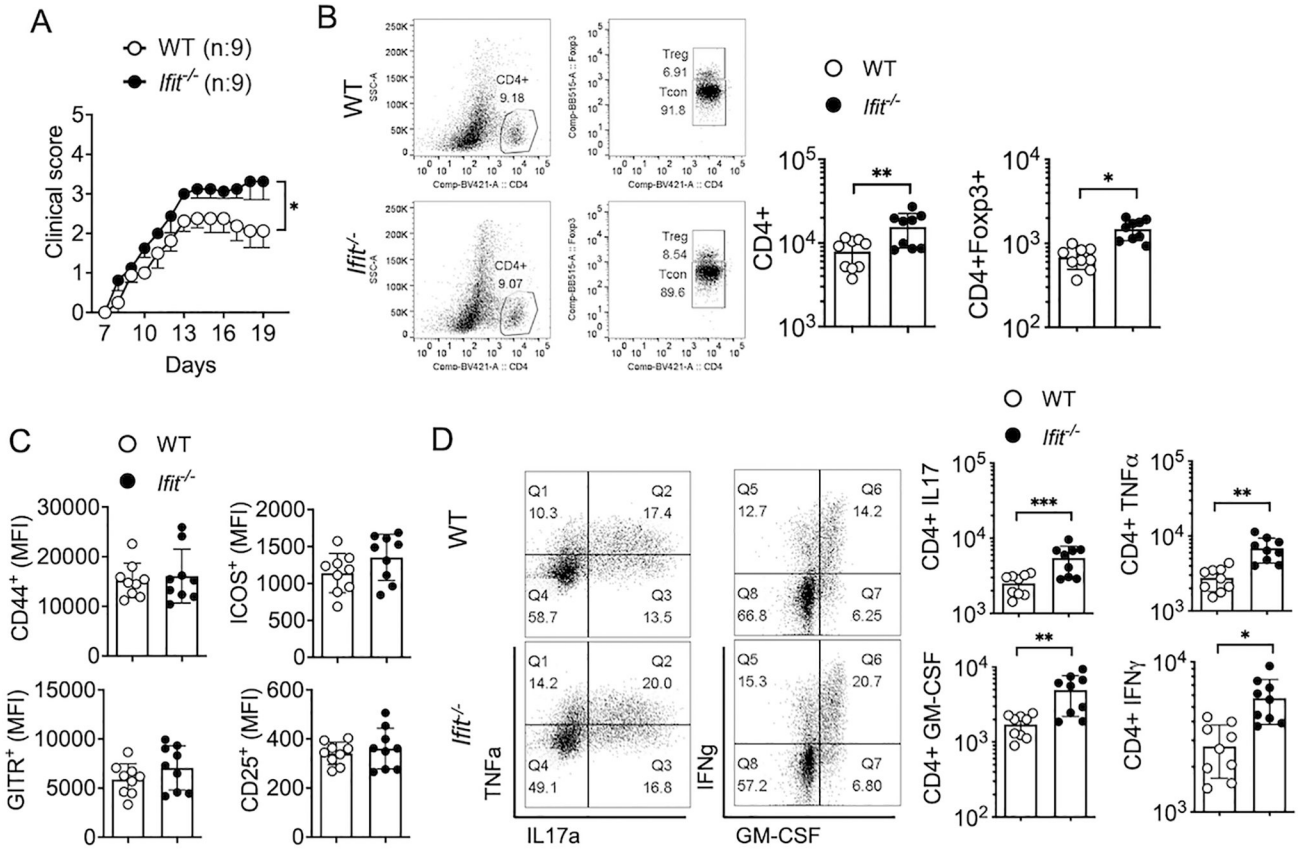

Fig 2. Increased susceptibility to EAE in *Ifit*$^{-/-}$ mice.

WT (n = 9) and *Ifit*$^{-/-}$ (n = 9) mice were induced for EAE. (**A**) EAE clinical score. (**B**) Absolute number of CNS-infiltrating CD4$^+$ T cells and CD4$^+$Foxp3$^+$ Treg cells in the CNS of WT and *Ifit*$^{-/-}$ mice at the peak of disease (day 17 post immunization). (**C**) The Mean Fluorescence Intensity (MFI) of CD44, ICOS, GITR and CD25 on CD4$^+$Foxp3$^+$ Treg cells in the CNS. (**D**) Total numbers of GM-CSF, IFNγ, IL-17, and TNFα expressing CD4$^+$ T cells infiltrating the CNS at the peak of disease (day 17 post immunization). The results shown are the mean ± SD of individually tested mice from two independent experiments. *p < 0.05; **p < 0.01; ***p < 0.001; as determined by Mann-Whitney nonparametric test.

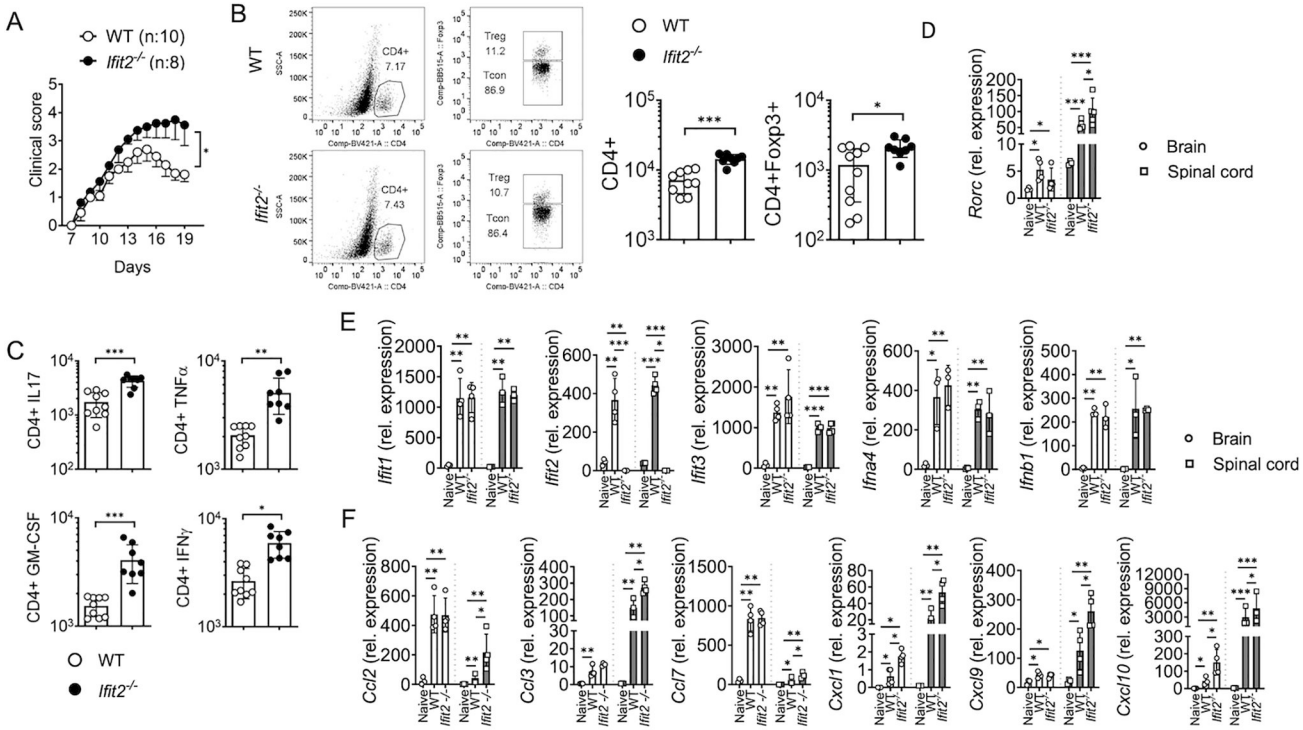

Fig 3. *Ifit2*$^{-/-}$ mice were more susceptible to EAE than WT mice.

WT and *Ifit2*$^{-/-}$ mice were induced for EAE. (**A**) EAE clinical score. (**B**) Absolute number of CNS-infiltrating CD4^{+} T cells and CD4^{+}Foxp3^{+} Treg cells in the CNS of WT and *Ifit2*$^{-/-}$ mice at the peak of disease (day 17 post immunization). (**C**) Numbers of GM-CSF, IFNγ, IL-17, and TNFα expressing CD4^{+} T cells infiltrating the CNS at the peak of disease (day 17 post immunization). n = 8–9 per group. (**D-F**) qPCR analysis of the indicated mRNAs in the brain and spinal cords from naïve, WT, and *Ifit2*$^{-/-}$ mice at the peak of disease (day 17 post immunization). n = 3–4 per group. The results shown are the mean ± SD of individually tested mice from two independent experiments. *p < 0.05; **p < 0.01; ***p < 0.001; as determined by Mann-Whitney nonparametric test.

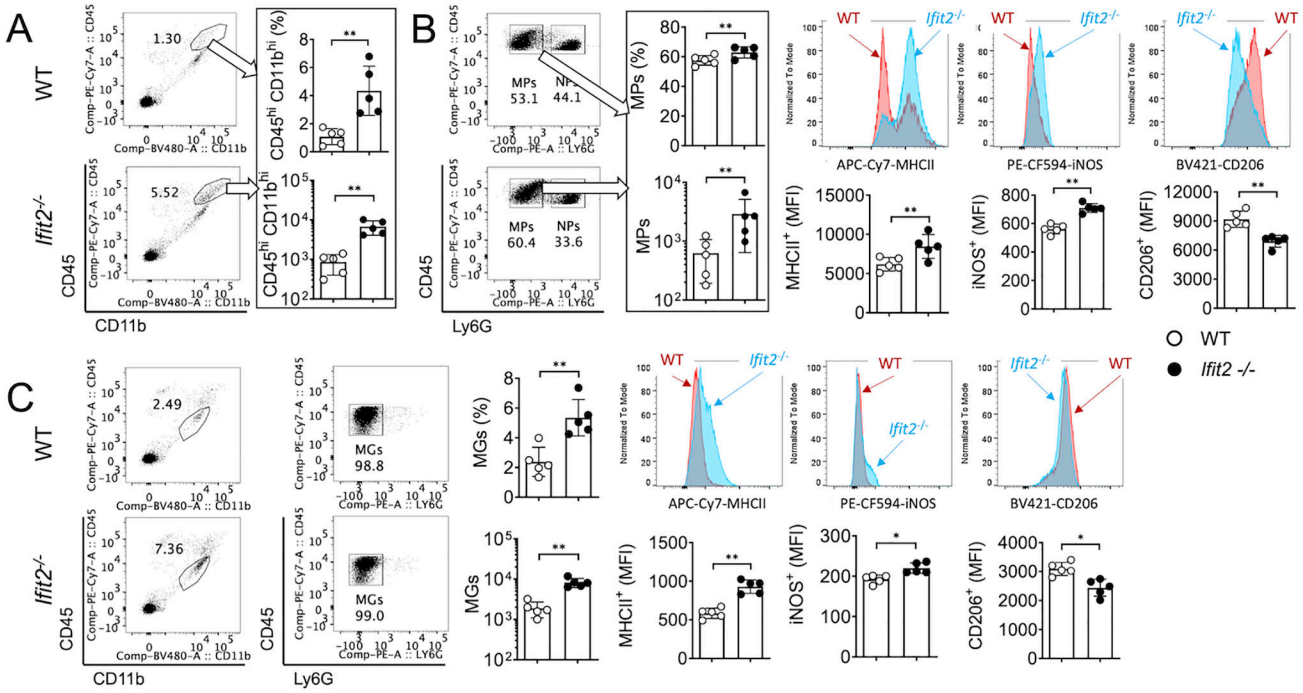

Fig 4. Phenotypes of myeloid subsets in the CNS of *Ifit2*$^{-/-}$ mice.

Representative flow cytometry plots of CD45^{high}CD11b^{high} cells (**A**) and of microglia (**C**) from CNS of WT and *Ifit2*$^{-/-}$ mice. (**B**) Neutrophils were excluded from CD45^{high}CD11b^{high} cells by Ly6G staining. Absolute numbers of infiltrating myeloid cells (Ly6G^{-}CD45^{hi}CD11b^{hi}) and microglia (CD45^{int} CD11b^{hi}) are shown. The Median Fluorescence Intensity (MFI) of MHCII, iNOS and CD206 expression measured by flow cytometry. The results shown are the mean ± SD of individually tested mice (n=5) from two independent experiments. *p < 0.05; **p < 0.01; ***p < 0.001; as determined by Mann-Whitney nonparametric test.

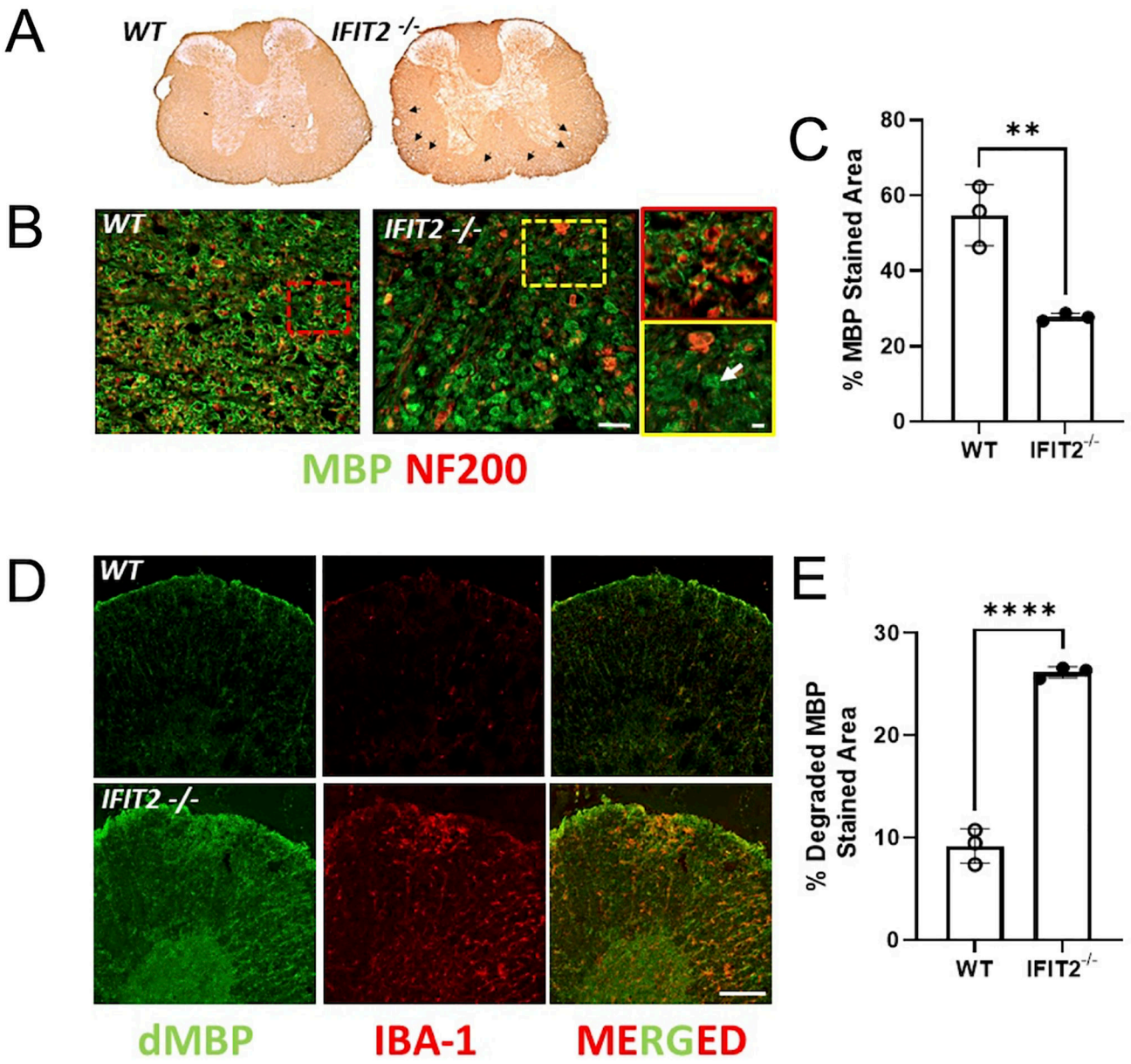

Fig 5. Demyelination in *Ifit2*$^{-/-}$ mice.

(**A**) Coronal cryosections of thoracic spinal cord of EAE induced WT and *Ifit2*$^{-/-}$ mice were stained with MBP and visualized by DAB, areas of demyelination are shown with black arrows, scale bar- 100μm. (**B**) In the WT and *Ifit2*$^{-/-}$ spinal cords, we performed double immunostaining with antibodies to Mbp showing myelin and NF200 showing axons to determine the status of demyelinated axons. Representative images showing co-localization of MBP (green) and NF (red) in EAE induced WT and *Ifit2*$^{-/-}$ at the peak of the disease in the thoracic spinal cord (scale bar-20μm). Enlarged images of WT (red) and *Ifit2*$^{-/-}$ (yellow) are shown in the inset with white arrow marking Mbp^{+} myelin sheath in *Ifit2*$^{-/-}$ mice that are devoid of NF200 labeled axons. (**C**) Quantification of percent MBP stained area in in WT and *Ifit2*$^{-/-}$ mice. (**D**) The *Ifit2*$^{-/-}$ mice show defective myelin debris clearance at the peak of EAE-induction. Representative co-immunostaining with antibodies to dMBP

(degraded MBP) (green) was used to assess myelin debris, microglia are shown with IBA-1 staining (red) (Scale bar-20μm). (**E**) Quantification of dMBP stained area in in WT and *Ifit2*$^{-/-}$ mice. All immunohistochemical staining were conducted in tissue collected from three independent experiments. Total 8 ROI/mice were analyzed for quantification. Average of each ROI/animal was used for generating the graphical data. **, $p<0.01$, ****, $p<0.0001$; determined by unpaired Student's t test.

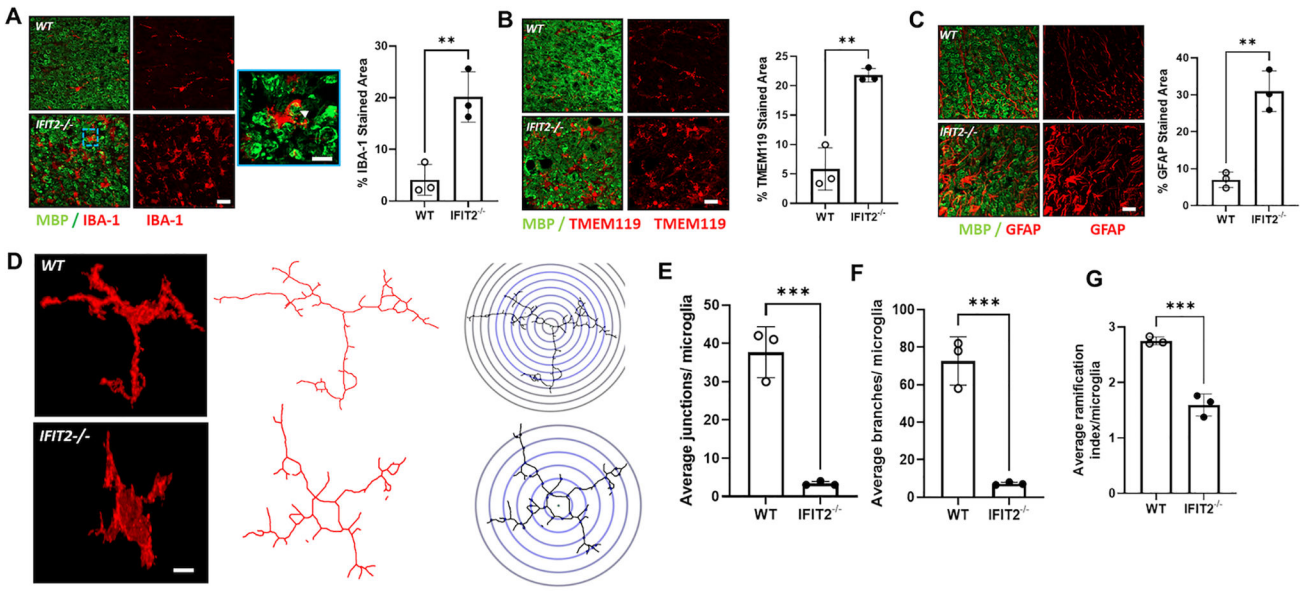

Fig 6. Ifit2 deficiency augments number of macrophage/microglia following EAE induction at the peak of disease.

Immunostaining of macrophage/microglia cell types in ventral white matter of thoracic spinal cord of WT and *Ifit2*$^{-/-}$ mice. (**A**) IBA-1 macrophage/microglia marker of inflammation (Scale bar: 20μm). Inset images showing engulfment of myelin debris by IBA1^{+} macrophage/microglia in cervical, thoracic, and lumbar regions (arrow, Scale bar: 5 μm). (**B**) Tmem119 staining, a marker of CNS local microglia in the ventral white matter of the thoracic spinal cord of WT and *Ifit2*$^{-/-}$ (Scale bar: 20μm). (**C**) Gfap staining for astrocytes in the ventral white matter of thoracic spinal cord of WT and *Ifit2*$^{-/-}$ mice (Scale bar: 20μm). (**D**) Representative images of microglia morphology in WT and *Ifit2*$^{-/-}$ cells (Scale bar: 5 μm). Quantification of microglial skeleton (red lines) and sholl analysis (circular in **D**) showing average junctions (**E**), branches (**F**) and ramification index (**G**). All immunohistochemical staining were conducted in tissue collected from three independent experiments. Total 8 ROI/mice were analyzed for quantification and average ROI measurement per animal was used for plots. **, p<0.01, ***, p<0.001; determined by unpaired Student's t test.

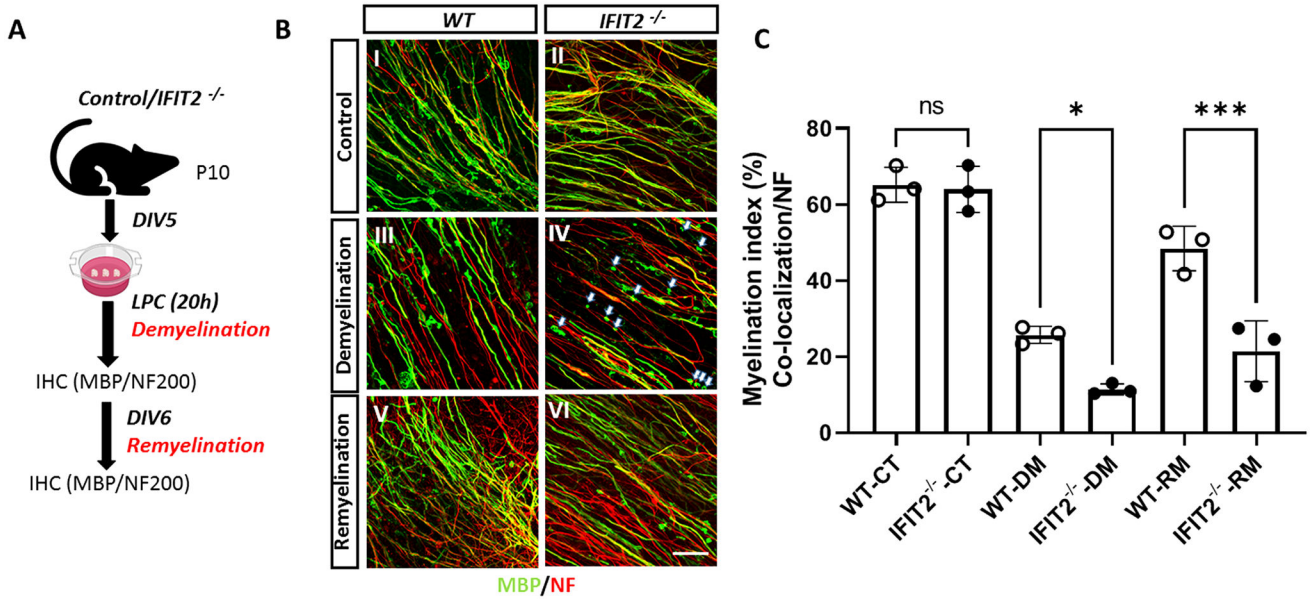

Fig 7. Ifit2 deletion is associated with increased demyelination, failed myelin debris clearance, and impaired remyelination.

(**A**) Organotypic slices from control and *Ifit2*$^{-/-}$ P10 mice were treated with lysolecithin (LPC) (0.5mg/ml) for 18 hrs to induce demyelination. Before treatment, brain organotypic sections from control (B.I) and *Ifit2*$^{-/-}$ (B.II) mice stained for myelin basic protein (Mbp) and axonal marker NF200. Compared to control slices (B.III), *Ifit2*$^{-/-}$ tissue section (B.IV) showed severe demyelination and lack of myelin clearance (white arrow in B.IV). Based on axonal staining, there was no drastic loss of axons between control and *Ifit2*$^{-/-}$ mice during demyelination. Following demyelination, the slices were allowed to recover and remyelinate for 7 days. Similar staining was carried out. Control slices (B.V) had significant recovery and remyelination. *Ifit2*$^{-/-}$ brain slices had significantly lower extent of remyelination (B.VI). (**C**) Quantification of myelination indices of each condition in comparison WT and *Ifit2−/−* cerebral slice culture (CT, control, DM, demyelinated, RM, remyelinated). All immunohistochemical staining were conducted in tissue collected from three independent experiments. Average myelination index data from 6 slices/brain were used in the plots between conditions. Scale bar: 20μm.***$p < 0.001$; *$p < 0.05$, determined by one way ANOVA.

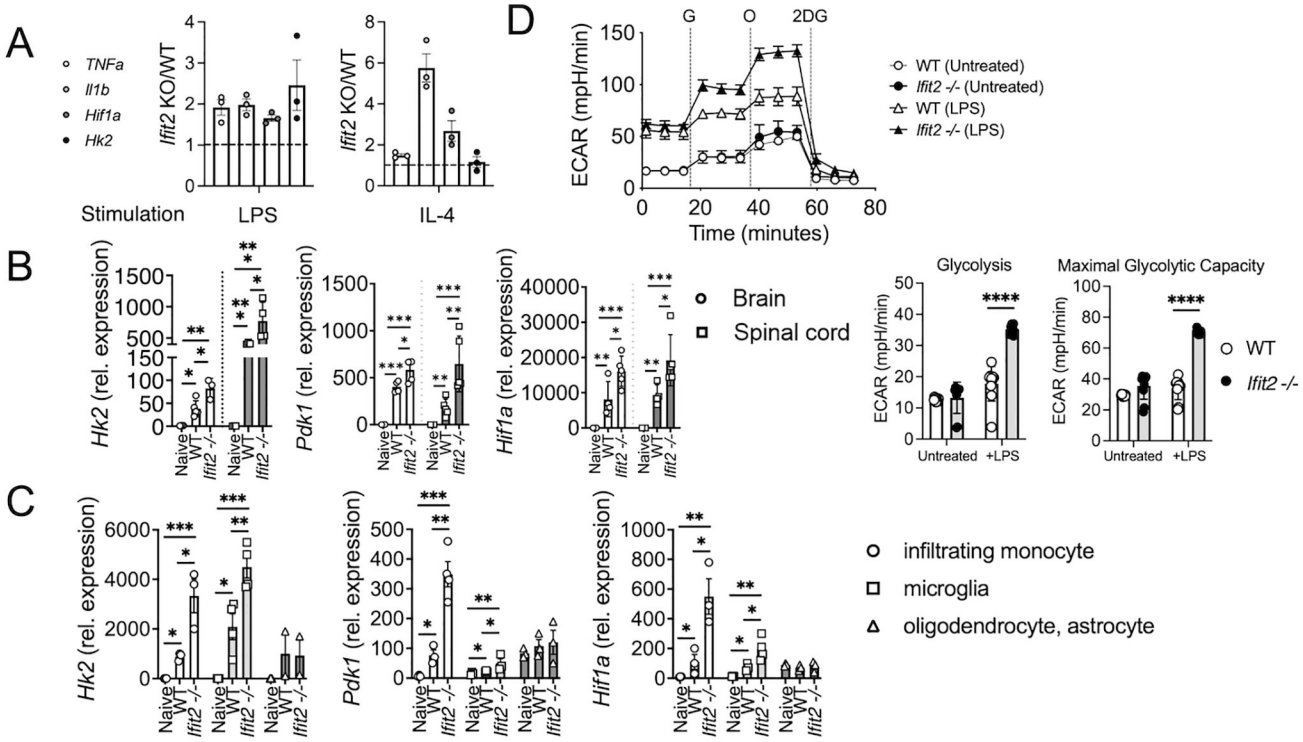

Fig 8. Cytokines and glycolytic gene expression in *Ifit2*$^{-/-}$ mice.

(**A**) mRNA expression of *Tnfa, Il1b, Hif1a, and Hk2* in bone marrow-derived macrophages from WT and *Ifit2*$^{-/-}$ mice were incubated with lipopolysaccharide (LPS; 1 μg/mL) or IL-4 (5000U/mL) for 48 h. n = 3 per group. (**B**) CNS tissues harvested at the peak of disease were measured for glycolytic gene (*Hk2*, *Pdk1*, and *Hif1a*) expression by qPCR. (**C**) Sorted CD45^{high} CD11b^{high} (infiltrating myeloid cells), CD45^{int} CD11b^{high} (microglia) and CD45^{low} (astrocyte and oligodendrocyte) cells from CNS of EAE induced mice (day 17 post immunization) and the indicated gene expression were measured by qRT-PCR. n = 3–4 per group. (**D**) BMDM cells generated were stimulated with LPS overnight and subjected to the Seahorse assay. Extracellular acidification rate (ECAR) is shown. The results shown are the mean ± SD of individually tested mice from two independent experiments. *, $p < 0.05$; **, $p < 0.01$; ***, $p<0.001$; ****, $p<0.0001$ as determined by Mann-Whitney nonparametric test.